

Article

Improvement of Electrical and Mechanical Properties of PLA/PBAT Composites Using Coconut Shell Biochar for Antistatic Applications

Justin George * , Daeseung Jung and Debes Bhattacharyya

Centre for Advanced Composite Materials, Faculty of Engineering, The University of Auckland, 314-390 Khyber Pass Road, Newmarket, Auckland 1023, New Zealand

* Correspondence: jgeo541@aucklanduni.ac.nz; Tel.: +64-273986178

Abstract: Biochar-based environment-friendly polymer composites are suitable substitutes for conventional non-biodegradable polymer composites. In this work, we developed polylactic acid (PLA)/polybutylene adipate-co-terephthalate (PBAT)/biochar (BC) composites with improved mechanical and electrical properties for antistatic applications. Coconut shell biochar was obtained through the pyrolysis of coconut shell in an inert atmosphere, and characterised using scanning electron microscopy (SEM), X-ray photoelectron spectroscopy (XPS) and X-ray diffraction (XRD), to investigate the morphology and structural properties. The biochar was converted to powder form, sieved to reduce the particle size ($\leq 30 \mu\text{m}$ diameters), and melt-mixed with PLA and PBAT to form composites. The composites were extruded to produce 3D printing filaments and, eventually, 3D-printed tensile specimens. The tensile strength and tensile modulus of the 3D-printed PLA/PBAT/BC (79/20/1) composite with 1 wt% of biochar improved by 45% and 18%, respectively, compared to those of PLA/PBAT (80/20). The interfacial interaction between the biochar and polymer matrix was strong, and the biochar particles improved the compatibility of the PLA and PBAT in the composites, improving the tensile strength. Additionally, the electrical resistivity of the composite did reduce with the addition of biochar, and PLA/PBAT/BC (70/20/10) showed the surface resistivity of $\sim 10^{11} \Omega/\text{sq}$, making it a suitable material for antistatic applications.

Keywords: polymer composites; biochar; pyrolysis; antistatic



Citation: George, J.; Jung, D.; Bhattacharyya, D. Improvement of Electrical and Mechanical Properties of PLA/PBAT Composites Using Coconut Shell Biochar for Antistatic Applications. *Appl. Sci.* **2023**, *13*, 902. <https://doi.org/10.3390/app13020902>

Academic Editor: Antonios Papadopoulos

Received: 9 December 2022

Revised: 3 January 2023

Accepted: 4 January 2023

Published: 9 January 2023



Copyright: © 2023 by the authors. Licensee MDPI, Basel, Switzerland. This article is an open access article distributed under the terms and conditions of the Creative Commons Attribution (CC BY) license (<https://creativecommons.org/licenses/by/4.0/>).

1. Introduction

Electrostatic charging is an issue for electronics (packing and transport), fuel tanks and equipment in explosive environments [1,2]. Electrostatic discharge (EDS) during assembling, packing and shipping causes severe economic loss [3]. Antistatic and electrostatic dissipative materials with surface resistivity ($< 1 \times 10^{12} \Omega/\text{sq}$) resolve this issue. There is a worldwide demand for antistatic and electrostatic discharge materials for electronic packing applications and personal protective equipment (PPE) used in hazardous explosive environments [4]. Carbon-based polymer composites are the most common antistatic materials, due to their favourable properties, including tuneable electrical conductivity, high thermal stability, chemical resistance and low photodegradation [5,6].

Several carbonaceous fillers, such as carbon black [7], carbon fibre, carbon nanotube [8] and graphene [9], improve the mechanical properties and electrical conductivity of the polymer matrix [10]. Such carbon-based composites find applications in electrostatic-dissipative and antistatic materials [11]. However, producing carbon-based conductive fillers requires petrochemical or non-renewable precursors, making them expensive and not environmentally friendly. It is essential to replace such electrically conductive reinforcing fillers with environmentally benign, cost-effective, renewable carbonaceous fillers [12,13]. A suitable substitute for petrochemical-based conductive fillers in the polymer matrix is biochar produced through biomass pyrolysis in an oxygen-deficient/inert atmosphere. The pyrolysis

of biomass in an inert atmosphere expels the volatiles from organic matter and produces carbon-rich residue with a porous structure [14,15]. However, the physical and chemical properties of the biochar depend on the precursor and the pyrolysis conditions applied. The pyrolysis of biomass at low temperatures (≤ 700 °C) contains a high concentration of functional groups and low carbon content [16]. However, if the pyrolysis is carried out at a higher temperature, in an oxygen-deprived atmosphere, it can improve the specific surface area and carbon content, especially the amount of sp^2 hybridised carbon, imparting electrical conductivity to the residual carbon [17,18]. Such biochar material with a high carbon content is thermally stable and porous, with a large surface area, allowing the infiltration of polymer materials into the pores, thus improving the interlocking of particles with polymer matrix [14,19,20]. Moreover, due to the low concentration of functional groups, biochar shows better compatibility with the polymer matrix, compared to natural fibres [21,22]. Biochar also has high thermal stability; hence, biochar composites can be processed at higher temperatures [23].

Coconut (*Cocos nucifera*) shell is an organic waste, abundantly present in Asian and South American countries [24,25]. It is a good precursor for producing activated charcoal and has recently been used to develop functional materials for contamination removal, energy storage, and for manufacturing reinforced polymer composites [26–30]. Although biochars from different precursors have proven to be suitable reinforcing fillers for polymer matrices such as poly(trimethylene terephthalate)/poly (lactic acid) (PTT/PLA) blend [31], polypropylene [14,32], poly(vinyl alcohol) (PVA) [23] and PLA/potato starch blend [33], studies on the utilisation of biochar composites as antistatic material are limited. For the application of antistatic personal-protective-equipment (PPE) and electronic packing material, both good electrical (surface resistivity $\leq 1 \times 10^{12}$ Ω /sq) and mechanical properties are essential. Moreover, personal protective equipment (PPE) and electronic packing material must be disposed of once damaged, or after use. Hence, the most important properties required for PPE in hazardous environments or packing materials for electronics are their suitable mechanical, electrical (antistatic) and biodegradability properties. Biochar produced at a high temperature through pyrolysis in an inert atmosphere shows electrical conductivity, due to a high concentration of sp^2 hybridised carbon content [34].

In this work, a blend of PLA and PBAT is used as the matrix for the biochar composite. PLA has a surface resistivity of 10^{13} – 10^{16} Ω /sq, while that of PBAT is $\sim 10^{16}$ Ω /sq [35]. PLA/PBAT blend is biodegradable and has improved ductility compared to PLA [36,37]. However, PLA and PBAT are immiscible, and exist as separate phases in the matrix. The blend also shows low electrical conductivity, and is unsuitable for antistatic applications [38]. However, incorporating conductive biocarbon-fillers can reduce the electrical resistivity of the composites. The nano- and micro-particle fillers improve the compatibility between the PLA and PBAT phases, by increasing the interfacial interaction of the PLA and PBAT domains. A combined improvement in both the electrical and mechanical properties of the composites is essential for antistatic material for any practical application. Hence, we attempt to improve the compatibility of the PLA/PBAT phases and electrical properties (antistatic properties) of the PLA/PBAT composites, using biochar. We envisage that the current work will open up an avenue for the development of sustainable biochar-based antistatic composites.

2. Materials and Methods

Poly(lactic acid) (PLA) 3D printing grade with trade name Ingeo BioPolymer 3D850 with a specific density of 1.24 g/cm³ and melt flow rate (MFR) of 7–9 g/10 min (ASTM D1238) in pellet form was supplied by NatureWorks LLC, Plymouth, MN, USA. PBAT (item code: CPLNA-03459 BLN0430015; item description: Renol 03459 PBAT CMP Natural) natural to off-white granules with a density of 1.27 g/mL at 20 °C (ISO 1183-1) and a melt flow index (190/2.16 °C/kg) of 4 g/10 min (ASTM D1238) was supplied by Clariant, Auckland, New Zealand. Coconut-shell biochar granules were produced by the pyrolysis of coconut shell at 800 °C in a nitrogen atmosphere at a heating rate of 10 °C/min and a

residence time of 30 min, using a tube furnace (SAF therm, Model: STG-100-17, Luoyang, China). Before mixing, the prepared biochar was dried, ground, sieved, and stored in a desiccator.

2.1. Characterisation of Biochar

The surface-morphology characterisation was conducted through scanning electron microscopy (Hitachi SU-70 FE-SEM, Hitachi High-tech, Ibaraki, Japan). The particle-size distribution and average particle size were calculated using Image J software from scanning electron micrographs of the biochar particles. The elemental analysis of the biochar was performed using X-ray photoelectron spectroscopy (Kratos Axis DLD XPS) with an area of analysis of 700 μm \times 300 μm and a spot size of 15 μm diameter and special resolution of <3 μm . The XPS data were analysed using CasaXPS[®] version 2.3.18 software. XRD analysis was carried out using Rigaku MiniFlex II Desktop Powder Diffractometer (Tokyo, Japan) using monochromatic Cu K α radiation (30 kV, 15 mA). The diffraction data of the biochar samples were collected in the 2 θ range of 10 to 60 $^\circ$, at a scanning rate of 1 $^\circ$ 2 θ /min.

2.2. PLA/PBAT/BC Composite Preparation

PLA/PBAT/BC composites were melt-mixed in different formulations of PLA (85%, 80%, 79%, 77.5%, 75%, 70% *w/w*), PBAT (10%, 15% and 20% *w/w*) and BC (1%, 2.5%, 5% and 10% *w/w*), Table 1, using a Brabender mixer (Plasti-Corder Lab-station, Duisburg, Germany). The biochar powder, PLA and PBAT were dried in an oven at 70 $^\circ\text{C}$ for 24 h, and weighed and premixed. The premixed PLA, biochar and PBAT were melt-mixed (50 cm^3 chamber) and kept at 200 $^\circ\text{C}$ for 5 min at a screw speed of 70 rpm/min. After mixing, the composites were pelletised using a pelletising mill (Model: IZ-120, Lab tech Engineering Company Ltd., Samut Prakan, Thailand).

Table 1. Composition details of the polymer composites.

Specimen	Constituent		
	PLA (wt%)	PBAT (wt%)	Biochar (wt%)
PLA/PBAT (80/20)	80	20	0
PLA/PBAT/BC (79/20/1)	79	20	1
PLA/PBAT/BC (77.5/20/2.5)	77.5	20	2.5
PLA/PBAT/BC (85/10/5)	85	10	5
PLA/PBAT/BC (80/15/5)	80	15	5
PLA/PBAT/BC (75/20/5)	75	20	5
PLA/PBAT/BC (70/20/10)	70	20	10

2.3. Filament Preparation and 3D Printing

The pellets were dried at 70 $^\circ\text{C}$ for 24 h before extruding the 3D printing filaments. A single-screw extruder (3devo, Utrecht, The Netherlands) was used to produce 3D printing filaments with a size of 1.75 mm in diameter (Figure 1). The 3D-printer-filament extruder had four heating zones, and temperatures at different zones were set to 190 $^\circ\text{C}$ (feeding zone 1), 194 $^\circ\text{C}$ (zone 2), 199 $^\circ\text{C}$ (zone 3) and 199 $^\circ\text{C}$ (die). The rotational speed was 3.5 rpm. The 3D printing of polymer composites was performed in the Tronxy D01 Bowden 3D printer (Shenzhen, China). The printing parameters such as nozzle temperature (220 $^\circ\text{C}$), infill (100%), printing speed (60 mm/s), bed temperature (65 $^\circ\text{C}$) and nozzle size (0.4 mm) were kept constant for all samples.

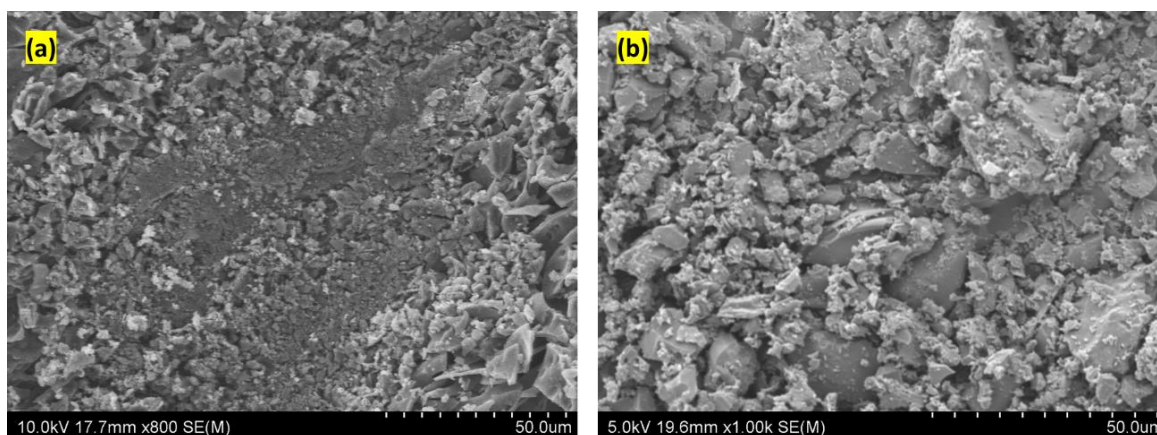


Figure 1. SEM images of biochar: (a) before, and (b) after size-reduction.

2.4. Characterisation of Composites and 3D-Printed Samples

The scanning electron microscope, Hitachi SU-70 FE-SEM was used for the surface morphology of the composites, the 3D-printed specimens and the tensile-fracture surfaces. All samples were coated with platinum, to avoid charging and increase secondary electron emission. A low acceleration voltage of 5 kV was used for secondary-electron SEM imaging.

2.4.1. Differential Scanning Calorimetry (DSC)

Differential-scanning-calorimetry (DSC) studies were performed using DSC Q 1000 (TA Instruments, New Castle, DE, USA). The heating was from 30 to 200 °C, and cooling was from 200 to 30 °C at a rate of 10 °C/min, with a holding time of 4 min; the samples were then heated again to 200 °C, before being tested using a heat-cool-heat cycle. The glass-transition, cold-crystallisation and melting temperatures were taken from the second heating-cycle. The purpose of the first heating-cycle was to eliminate thermal history. The crystallinity of the composites was calculated using the equation $X_c(\%) = \frac{\Delta H_m - \Delta H_{cc}}{\varphi \Delta H_m^0} \times 100$ [39,40], where the ΔH_m was the measured melting-enthalpy, ΔH_{cc} was the enthalpy of cold crystallisation, ΔH_m^0 was the melting enthalpy of 100% crystalline PLA (93.7 J/g from the literature), and φ was the weight fraction of PLA in the composites [39,41].

2.4.2. Thermogravimetric Analysis (TGA)

Thermogravimetric analysis (TGA) of the 3D printing filaments was carried out using TGA Q 5000 (TA Instruments, New Castle, DE, USA). The temperature program was set from 30 to 700 °C at a 10 °C/min heating rate, under a nitrogen atmosphere with a 50 mL/min nitrogen flow rate.

2.4.3. Attenuated Total Internal Reflectance Fourier Transform Infrared Spectroscopy (ATR-FTIR)

Attenuated total internal reflectance–Fourier-transform infrared spectroscopy (ATR-FTIR) of the composite was carried out using a Thermo-Scientific Nicolet iS50 FT-IR (Thermo Fisher Scientific Inc., Madison, WI, USA) with a diamond micro-tip accessory; an average number of 32 scans were taken in the wavenumber ranging from 400–4000 cm^{-1} .

2.4.4. Mechanical Testing and Electrical-Resistivity Measurement

The mechanical testing was conducted on an Instron 5567 (Norwood, MA, USA) under ambient conditions, following the ASTM D 638 protocol. Five type-IV specimens were 3D printed for the studies, with an infill of 100% and a nozzle temperature of 220 °C. A video extensometer was used to measure the extension. Electrical-resistivity measurements of the composites were carried out using a Keithley resistive meter 6517A, according to ASTM D257.

3. Results and Discussion

3.1. Biochar Structure and Morphology

Figure 1 displays the scanning-electron-microscope images of coconut shell biochar produced through the pyrolysis of coconut shell at 800 °C in an inert atmosphere. The figure shows that the biochar particles form irregular shapes with sharp edges, after size reduction, Figure 1b. In order to avoid clogging of biochar particles during printing, the particles were sieved using a 400 mesh-size.

The XPS survey spectra, Figure 2, reveal that the major elements present in biochar are carbon (~93.54%) and oxygen (~6.46%) without any significant impurities. Here, the high-resolution C1s quantitative spectra of biochar (inset of Figure 2) show a binding energy peak at 284.4 eV, corresponding to sp^2 hybridised carbon. Moreover, the deconvolution of the C1s peak reveals peaks at ~285.2 eV, attributed to an epoxy group (C-O-C), and at ~289.3 eV, corresponding to a carbonyl group (C=O). The percentages of epoxy and carbonyl groups were calculated as 31.83% and 17.65%, respectively. A major contribution to the total percentage was sp^2 hybridised carbon, of ~50.52%, which was much higher than sp^2 hybridised carbon in biochar produced at lower temperatures [42]. In this work, the coconut shell biochar showed a higher carbon content with a high purity, compared to those in other precursors and pyrolysis conditions. For example, rice husk biochar contains silicon dioxide as an impurity, while date palm biochar produced at 900 °C has a lower carbon concentration with impurities, when compared to the value for coconut shell biochar [18,42,43].

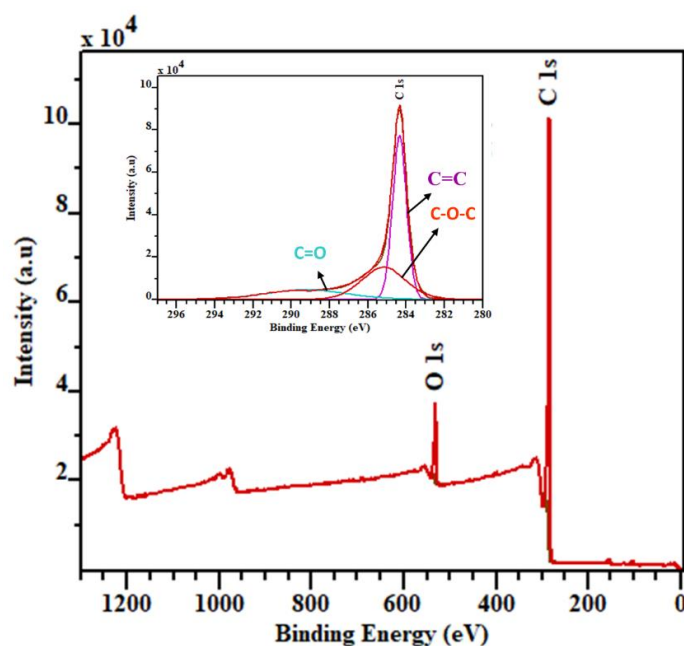


Figure 2. X-ray photoelectron spectra of coconut shell biochar.

The coconut-shell-biochar-powder crystallographic structure was determined through XRD analysis, Figure 3, which was performed in the range of 2θ angle from 10 to 60°. The broad peaks at $2\theta = 24.9^\circ$ and 43.4° correspond to the reflections from (002) and (100) planes in the disordered amorphous carbon structures. The sharp peak at 26.5° in the (002) plane is attributed to the ordered graphitic structures [44]. The coconut shell pyrolysis at 800 °C in an inert atmosphere favoured the formation of graphitic structure along with amorphous carbon, due to the peculiar pyrolysis conditions. Several other studies have shown that the biochar produced from other precursors and with other pyrolysis conditions favour the production of amorphous carbon over graphitic carbon [45–47]. According to Umerah et al., coconut shell carbon produced through autogenic pressure pyrolysis at a

pyrolysis temperature of 800 °C promoted the production of amorphous carbon which was verified through XRD analysis [33].

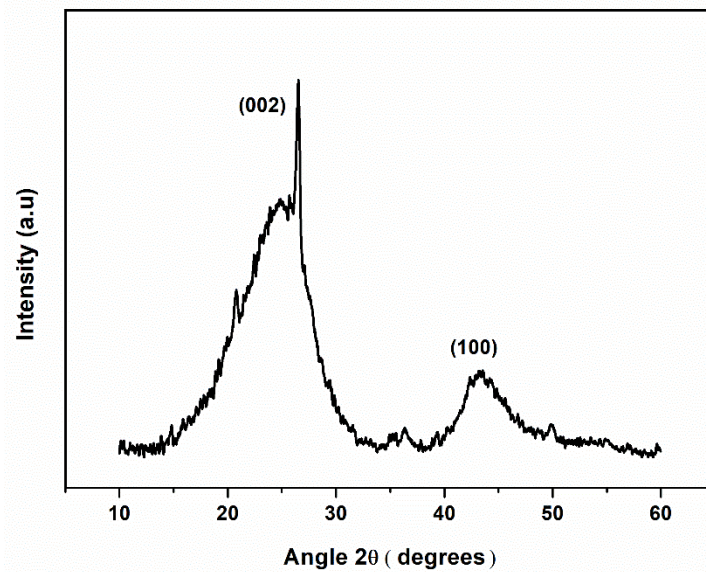


Figure 3. XRD pattern of coconut shell biochar.

3.2. Biochar Composites Characterisation

3.2.1. Thermal Behaviour of the PLA/PBAT/BC Composites

Figure 4 represents the DSC thermograms from the second heating-cycle of the PLA/PBAT blend and PLA/PBAT/BC composites. Here, two distinct transitions are observed: the cold-crystallisation exotherm at ~101.5 °C and a melting endotherm at ~176 °C for PLA/PBAT blend. The glass transition of the PLA/PBAT blend and composites appear around ~65 °C. The biochar addition into the PLA/PBAT blend decreases the cold-crystallisation temperature of the composites by (~5 °C) with 1 wt% of biochar content. Moreover, the crystallinity of neat PLA improves with filler addition, where fillers act as nucleating agents. These nucleating agents lower the cold-crystallisation temperature and improve the percentage crystallinity of PLA [48]. In PLA/PBAT/BC composites, the decrease in cold-crystallisation temperature can be attributed to the nucleation effect of the biochar particles, something which has also been observed in other biochar-based polymer composites [45,49].

Table 2 shows the thermal properties of the PLA/PBAT blend and PLA/PBAT/BC composites. The melting temperature (T_m), crystallisation temperatures (T_c) and total crystallinity (X_c) of the blend and composites have been calculated. The PLA/PBAT (80/20) blend has a melting point of 176.05 °C. It should be noted that adding even 1 wt% of biochar increases the composites' melting point by ~2 °C. The increase in melting temperature of the composite is due to an increase in the growth of the PLA crystalline phase [50]. However, introducing biochar into the PLA/PBAT blend dramatically improved the percentage crystallinity of the composites by ~40.6% in PLA/PBAT/BC (85/10/5), compared to that of the PLA/PBAT (80/20) blend. As expected, the total crystallinity also decreased as the PLA content in the composite decreased (Table 2). A high concentration of PBAT in the PLA/PBAT blend reduced the crystal nuclei number and spherulite growth rate, leading to a decline in the degree of crystallinity [51]. Moreover, the lowering of crystallinity in PLA/PBAT composites with the increase in PBAT may be attributed to the low crystallinity of PBAT. Furthermore, the phase separation of PLA and PBAT restricted the PLA-polymer-chain alignment [52], although adding biochar into the PLA/PBAT blend improved the total crystallinity of the composites.

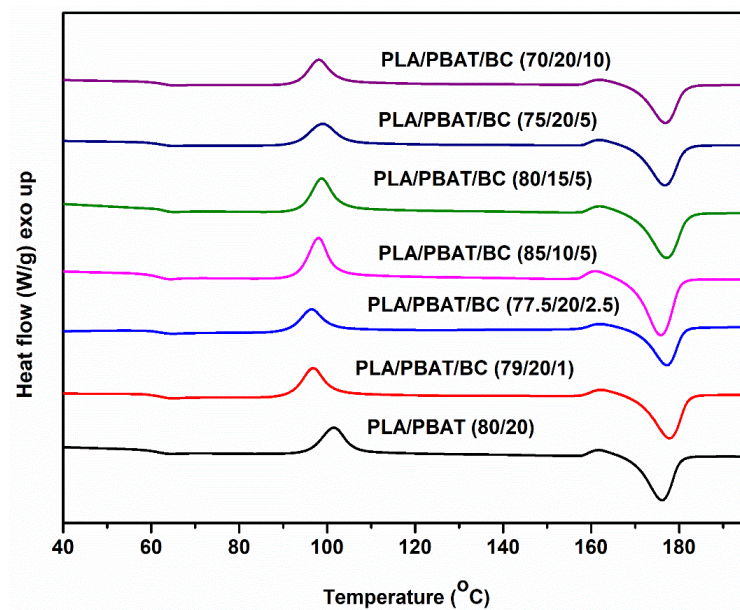


Figure 4. DSC of PLA/PBAT/BC composites.

Table 2. Thermal properties of the PLA/PBAT/BC composites.

Material	T_c [°C]	T_m [°C]	ΔH_{cc} [J/g]	ΔH_m [J/g]	X_c [%]
PLA/PBAT (80/20)	101.54	176.05	17.41	34.30	22.53
PLA/PBAT/BC (79/20/1)	96.76	177.77	18.17	36.63	24.93
PLA/PBAT/BC (77.5/20/2.5)	96.50	177.23	16.54	38.27	29.92
PLA/PBAT/BC (85/10/5)	98.03	177.86	20.72	44.47	31.68
PLA/PBAT/BC (80/15/5)	98.76	176.90	17.05	38.76	28.96
PLA/PBAT/BC (75/20/5)	99.01	176.76	17.71	36.85	27.23
PLA/PBAT/BC (70/20/10)	98.03	176.82	15.75	36.12	31.05

Figure 5 depicts the TGA and DTG of the PLA/PBAT/BC composites. Table 3 summarises the onset of degradation temperature (T_5 , a temperature at which 5 wt% degradation occurs), maximum degradation (T_{max}) and percentage of char formed at 550 °C. Thermal degradation mainly appears between 300 °C and 500 °C, because of two main constituents. The first weight loss corresponds to PLA, and the second to the PBAT between 400 °C and 450 °C [53]. The biochar in the composites is thermally stable, and shows no degradation even at 600 °C, which is expected, as the pyrolysis temperature was 800 °C. The char-residue percentage at 550 °C (Table 3) confirms the content of biochar in the composites.

The onset of degradation (T_5) and the maximum degradation temperatures of different composites are shown in Table 3. The onset of degradation started at 346.98 °C for PLA/PBAT (80/20) and moderately improved, with an increase in PBAT and biochar content, reaching a maximum of 351.45 °C for PLA/PBAT/BC (70/20/10). Unlike in the biochar poly(propylene) composites, the onset of degradation does not show any considerable improvement with biochar addition; this is crucial in determining the nozzle temperature for the 3D printing process [39]. A suitable printing temperature (220 °C) was used without nozzle clogging and degradation. The 3D-printing-nozzle temperature of 220 °C was safer, since this was much lower than the onset of degradation of the PLA/PBAT blend and the PLA/PBAT/BC composites. Another critical piece of information is the percentages of char residue at 550 °C, which for the PLA/PBAT blend was only 1.37%, but was around 5.38% for composites with 5 wt% biochar, while for composites with 10 wt% of biochar it was ~12.95%. Therefore, it appears that the char residue of the composites mainly depends on the amount of biochar added to them [39].

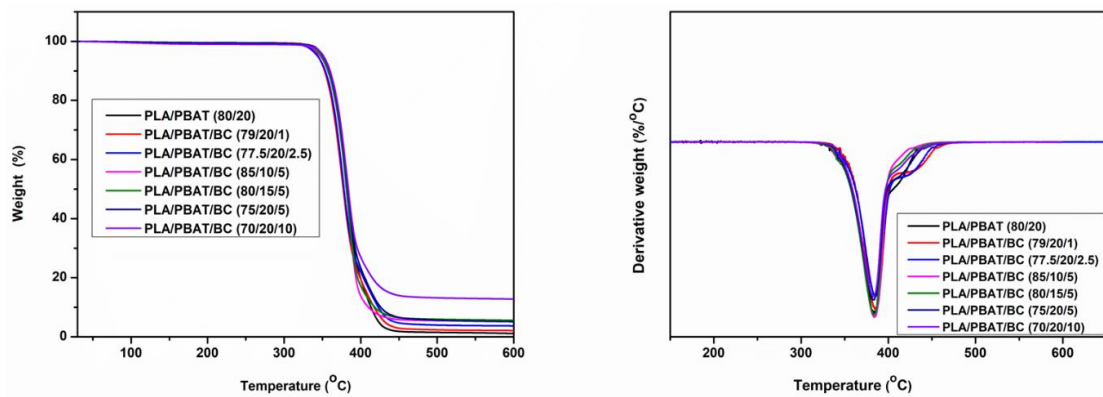


Figure 5. TGA analysis of biochar composites.

Table 3. The onset of degradation temperature (T_5), the temperature of maximum degradation (T_{max}) and char residue (%) at 550 °C.

Samples	T_5 (°C)	T_{max} (°C)	Char Residue at 550 °C (%)
PLA/PBAT (80/20)	346.98	382.86	1.37
PLA/PBAT/BC (79/20/1)	346.21	383.93	2.27
PLA/PBAT/BC (77.5/20/2.5)	346.50	384.12	3.53
PLA/PBAT/BC (85/10/5)	347.49	384.69	5.38
PLA/PBAT/BC (80/15/5)	348.62	383.58	5.70
PLA/PBAT/BC (75/20/5)	351.04	382.58	5.33
PLA/PBAT/BC (70/20/10)	351.45	382.07	12.95

3.2.2. ATR-FTIR Analysis of the Biochar Composites

A broad absorption peak around 3200–3600 cm^{-1} , Figure 6, corresponds to stretching vibrations of the hydroxyl (O–H) group. The peaks around 2800–3000 cm^{-1} are associated with symmetric stretching vibrations of C–H groups. Three peaks in the range of 1300–1500 cm^{-1} correspond to vibrations of C–H in CH_3 groups. An intense peak at 1710–1720 cm^{-1} corresponds to the carbonyl group (C=O) [54]. As the biochar production is through the pyrolysis of the biomass at a high temperature (800 °C), the percentage of functional groups is expected to be less; hence, no significant difference in the composite peaks occurs with the addition of biochar. Comparing the FTIR spectra of the PLA/PBAT (80/20) blend and PLA/PBAT/BC (75/20/5) composite show no peak changes due to biochar, indicating that mixing is purely physical. These results are consistent with previous studies [18,55].

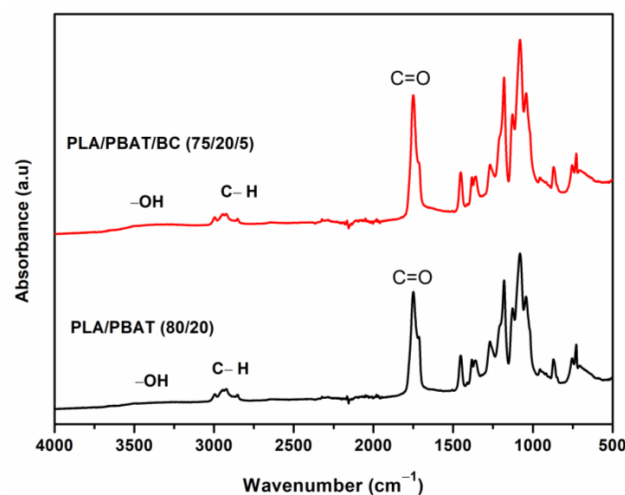


Figure 6. FTIR of PLA/PBAT blend and PLA/PBAT/BC (75/20/5) composite.

3.2.3. Electrical Properties of PLA/PBAT/BC Composites

In many industries (petrochemical, mining or power industries), personal protective equipment (PPE) is used in a dangerous explosive atmosphere. The main reason for the explosion is the charges accumulated on the surface of such PPE. Hence, it is desirable to use electrostatic dissipative, durable, sustainable and environment-friendly materials for such applications. The surface resistivity of the PLA/PBAT blends modified with different concentrations of biochar is shown in Table 4. When the biochar content in the composites increases from 0 wt% to 10 wt%, surface resistivity decreases by two orders of magnitude. Compared to other carbon-based composites, the decrease in electrical resistivity is not so drastic; however, the composite with 10 wt% of biochar shows a surface resistivity of $\sim 10^{11} \Omega/\text{sq}$, which is lower than the previously reported value ($3 \times 10^{12} \Omega/\text{sq}$ with 10 wt% of biochar) in the PLA/PBAT/biochar composites [3,56]. This low electrical resistivity is due to the high concentration of sp^2 hybridised carbon in coconut shell biochar. However, the presence of functional groups and impurities may reduce the electrical conductivity of the biochar particles. Moreover, biochar particle-size, shape and orientation play major roles in attaining a continuous conductive network in the polymer matrix. It is worth noting that PLA/PBAT/BC (70/20/10) shows conductivity in the range of antistatic material [57] making it suitable as 3D-printing material or film for packing, to prevent surface charge-accumulation. The packing material with surface resistivity of $1 \times 10^{11} \Omega/\text{sq}$ is sufficient for maintaining the static-dissipative properties [56,58]. Previous electrical studies have demonstrated that biochar can be a potential material for electrical applications. However, the electrical conductivity of biochar depends on the amount of sp^2 hybridised carbon content and a low concentration of impurities [18,59,60]. Coconut shell biochar produced at 800 °C has a high sp^2 carbon content and negligible impurities, making it a suitable filler material for antistatic PLA/PBAT composites.

Table 4. Surface resistivity of PLA/PBAT/BC composites.

Material	Surface Resistivity (Ω/sq)
PLA/PBAT (80/20)	1.58×10^{13}
PLA/PBAT/BC (79/20/1)	4.70×10^{12}
PLA/PBAT/BC (77.5/20/2.5)	2.72×10^{12}
PLA/PBAT/BC (85/10/5)	2.592×10^{12}
PLA/PBAT/BC (80/15/5)	2.23×10^{12}
PLA/PBAT/BC (75/20/5)	2.1×10^{12}
PLA/PBAT/BC (70/20/10)	1.03×10^{11}

3.3. Characterisations of 3D-Printed Specimens

Figure 7 shows the SEM images of the tensile fractured surface of the PLA/PBAT/BC composites. The phase separation of the PLA and PBAT blends is due to their immiscibility, which has been reported elsewhere [61]. The PLA/PBAT (80/20), Figure 7a, and PLA/PBAT/BC (79/20/1), Figure 7b, show a fibre-like structure, indicating the plastic deformation of the polymer matrix. The PBAT phase is ductile and elongated during tensile testing. Figure 7a shows a weak interfacial-interaction of the PBAT phase (marked with red arrows) with the PLA phase, as observed in the PLA/PBAT (80/20) blend [62]. However, such phase separation is not visible in Figure 7b; PLA/PBAT/BC (79/20/1) shows a better interfacial-interaction between PLA and PBAT in the presence of biochar. The presence of PBAT is favourable for improving the impact-resistance behaviour of PLA/PBAT blends [40]. However, the compatibility of the PLA and PBAT phases is essential for improving tensile properties. A weak interfacial-bonding between the PLA and PBAT phases lowers the tensile strength of the blend. When the biochar concentration is low (1 wt%), the droplet structure disappears, and a continuous matrix with elongated fibres is observed, Figure 7b. Moreover, biochar particles are wrapped with the polymer blend, indicating a strong bonding of biochar with the polymer matrix. The interfacial region of the biochar polymer matrix indicates a strong bonding between the polymer matrix and the biochar

particles, Figure 8. However, the fibril structure disappears when the PLA/PBAT blend is reinforced with biochar at a higher concentration (10 wt%), Figure 7d, indicating the increase in brittleness of the composite with a high biochar-loading. The dispersion and size of the separated domain depend on many factors, such as processing condition, constituent ratio and interfacial tension [40]. The PBAT phase is well dispersed, with better interfacial interactions between PLA and biochar in PLA/PBAT/BC (79/20/1) and PLAPBAT/BC (77.5/20/2.5) composites.

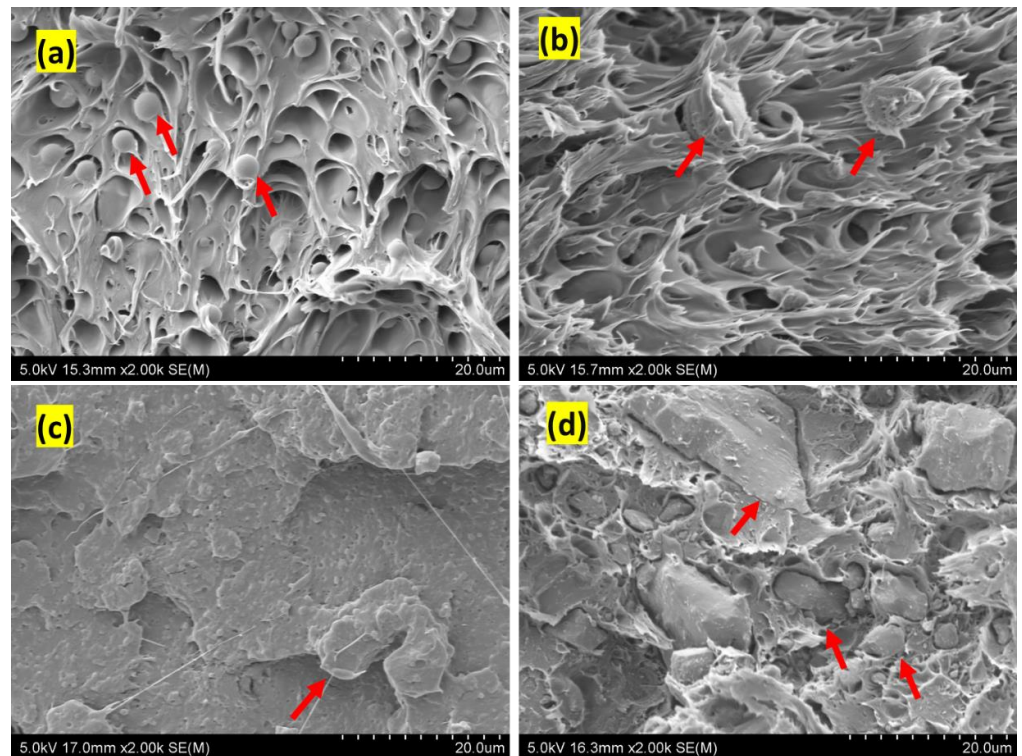


Figure 7. SEM images of fractured surfaces: (a) PLA/PBAT (80/20) (b) PLA/PBAT/BC (79/20/1) (c) PLA/PBAT/BC (77.5/20/2.5) and (d) PLA/PBAT/BC (70/20/10). [The red arrow in (a) shows the PBAT phase in the PLA matrix and (b–d), biochar particle].

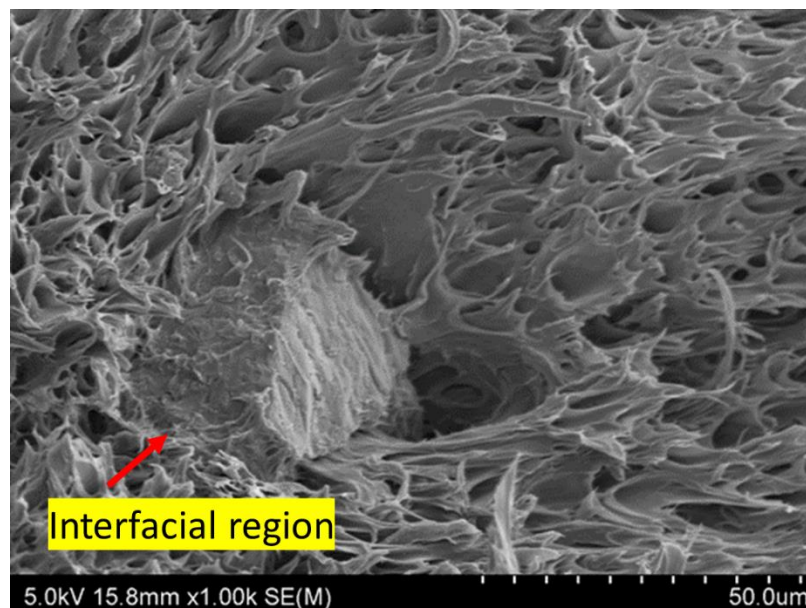


Figure 8. Interfacial region of biochar and PLA/PBAT in PLA/PBAT/BC (79/20/1).

A smaller domain size of the dispersed phase indicates low interfacial-tension between PLA and PBAT, Figure 7c. The lower interfacial-tension permits a larger surface area, allowing the large drops to split into smaller droplets [61]. Moreover, the biochar particles are covered with a polymer matrix, indicating a greater affinity of the polymer with coconut shell biochar. The interfacial interaction between the biochar and PLA/PBAT blend and the disappearance of droplet structure indicates that a low biochar concentration (1 wt%) improves the compatibility of PLA and PBAT.

3.4. Toughening Mechanism of the Composites

Studies have shown that the micro and nanoparticles improve the compatibility between the PLA and PBAT phases [63,64]. The carbon nanotubes introduced into the PLA and PBAT blend shows a greater affinity towards the PBAT phase; however, they make protrusions into the PLA phase, which acts as a bridge between the PLA and PBAT phases. The strong affinity of the carbon nanotubes to PBAT is due to the presence of aromatic molecules in PBAT, and the fact that carbon nanotubes prefer aromatic molecules [38,65]. Similarly, in PLA/PBAT/biochar composites, the interfacial interaction of biochar and the polymer matrix is strong, and the biochar particles are wrapped with polymer material, indicating a greater affinity of the biochar with the polymer matrix and an improvement in the compatibility of the polymer phases. The biochar particles in the interface between the PLA and PBAT matrix improve the compatibility between the polymer phases and the mechanical properties of the composite, as illustrated in Figure 9.

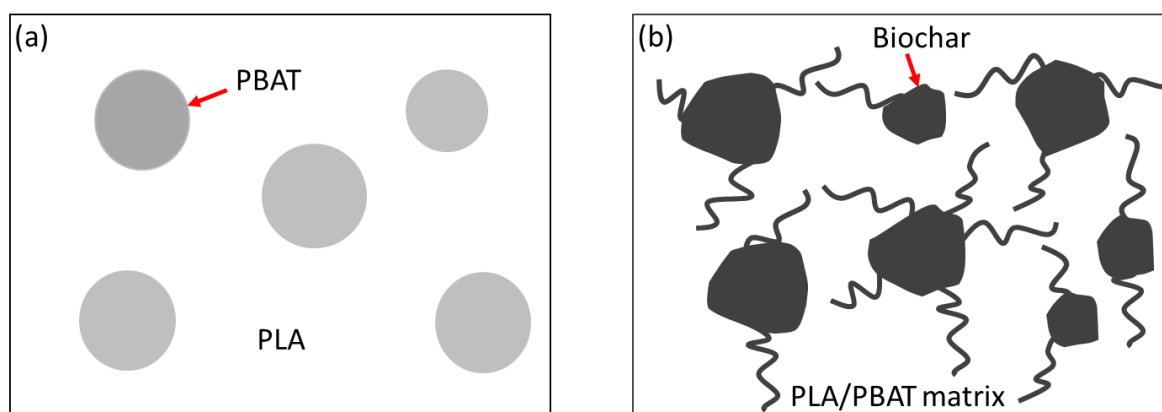


Figure 9. Schematic diagram of (a) phase-separated PLA/PBAT blend and (b) biochar polymer matrix interaction in PLA/PBAT/biochar composites.

Mechanical Properties of the 3D-Printed Composites

Combined mechanical and antistatic properties are essential for an antistatic personal-protective-equipment (PPE) and packing application. Figure 10 depicts the tensile properties of the PLA/PBAT blend and PLA/PBAT/BC composites. The results show that with a small concentration of biochar (1 wt%), the PLA/PBAT/BC (79/20/1) composite shows the highest tensile strength, with the maximum mean value of 42.3 MPa, while the (70/20/10) composite shows the lowest mean value of 24.62 MPa, with 10 wt% of biochar, Figure 10.

The improvement of the tensile strength of the composite with biochar may be attributed to the increased interfacial-interaction between the biochar and polymer matrix, which is evident in the SEM analysis. The biochar particles can divert part of the stress from the polymer matrix, and obstruct crack formation [66]. Furthermore, biochar improves the compatibility of the PLA and PBAT phases and the interfacial interaction between these polymer phases. Moreover, biochar increases the composites' total crystallinity by improving the crystallinity of the PLA [67]. As discussed earlier, the crystallinity of the composites improves, due to the nucleation effect of the biochar particles. However, the agglomeration behaviour becomes dominant at high concentrations of biochar, leading to decreased tensile-strengths [38,68]. Comparing the tensile moduli of the blend and the

composites, there is only a slight change. In addition, elongations at yield of the composites and blend remain almost the same with different biochar and polymer-blend compositions.

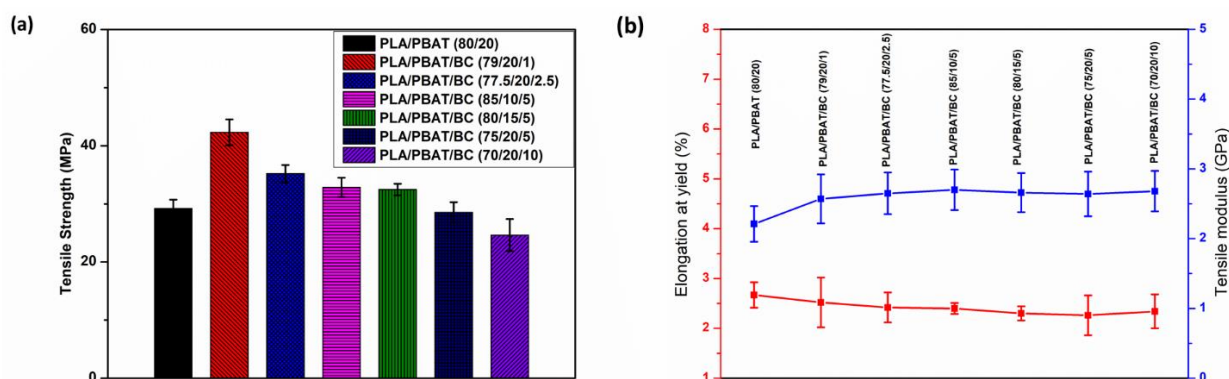


Figure 10. (a) tensile strength, (b) tensile modulus and elongation at yield of the composites.

4. Conclusions

Coconut shell biochar-incorporated PLA/PBAT polymer composites show improvements in mechanical and electrical properties (surface resistivity $\sim 10^{11} \Omega/\text{sq}$) and are suitable for antistatic application (antistatic material). Antistatic property can be achieved for the composite with a low biochar-loading concentration (10 wt%) instead of the previously reported 30 wt% of wood-biochar addition for antistatic PLA/PBAT composites. The XRD and XPS studies on coconut shell biochar reveal that it contains high carbon content with sp^2 hybridised graphitic carbon, improving the conductivity of the filler particles. The presence of highly pure carbon without impurities, a low percentage of functional groups, and reduced particle-size are beneficial for improving the electrical properties of the composites. TGA and DSC analyses show that the biochar composites are thermally stable, and the biochar particles act as nucleating agents, promoting PLA crystallisation. The tensile strength of the 3D-printed specimens with 1 wt% of biochar, PLA/PBAT/BC (79/20/1), shows the highest average value of 42.3 MPa. However, the tensile modulus and elongation at yield remain steady without appreciable change. The interfacial interaction of the biochar and polymer matrix studied using SEM reveals that the biochar has a strong interaction with the polymer matrix, possibly due to the low concentration of functional groups associated with the biochar particles. Here, biochar improves the compatibility of the PLA and PBAT phases, improving the composite's mechanical properties, especially the tensile strength. Furthermore, the electrical resistivity of the composites decreases with the addition of biochar, and the composite with 10 wt% of biochar shows a surface resistivity of $\sim 10^{11} \Omega/\text{sq}$, without any significant reduction in mechanical properties, making it a suitable antistatic material for packaging applications or personal protective equipment (PPE). Hence, the coconut shell biochar-filled PLA/PBAT composite is a suitable sustainable, environment-friendly, low-cost material for antistatic applications. Further studies on the improvement of the electrical properties of the biochar filler (with optimised pyrolysis conditions) and the effects of nano-sized biochar particles on the electrical and mechanical properties, are being conducted.

Author Contributions: J.G.: conceptualization, methodology, formal analysis, writing—original draft preparation. writing—review and editing. D.J.: writing—review and editing. D.B.: resources, supervision, funding acquisition, validation, writing—review and editing. All authors have read and agreed to the published version of the manuscript.

Funding: Ministry of Business, Innovation & Employment, New Zealand, for their financial support (grant number: UOA 3706657).

Institutional Review Board Statement: Not applicable.

Informed Consent Statement: Not applicable.

Acknowledgments: The authors thank all technicians at the Centre for Advanced Composites Materials (CACM) for their assistance. In addition, the authors would like to acknowledge the Ministry of Business, Innovation & Employment, New Zealand, for their financial support (grant number: UOA 3706657).

Conflicts of Interest: The authors declare no conflict of interest.

References

1. Radgowski, E.; Albrecht, R. Investigation of electrostatic discharge in aircraft fuel tanks during refueling. *J. Aircr.* **1979**, *16*, 506–512. [[CrossRef](#)]
2. Krein, P.T. Electrostatic discharge issues in electric vehicles. *IEEE Trans. Ind. Appl.* **1996**, *32*, 1278–1284. [[CrossRef](#)]
3. Galembeck, F.; Al Burgo, T. Accidents and losses caused by electrostatic discharge. In *Chemical Electrostatics*; Springer: Berlin/Heidelberg, Germany, 2017; pp. 169–183.
4. Jachowicz, M. Electrostatic Properties of Selected Personal Protective Equipment Regarding Explosion Hazard. *J. Sustain. Min.* **2013**, *12*, 27–33. [[CrossRef](#)]
5. Ghasemi-Kahrizsangi, A.; Shariatpanahi, H.; Neshati, J.; Akbarinezhad, E. Degradation of modified carbon black/epoxy nanocomposite coatings under ultraviolet exposure. *Appl. Surf. Sci.* **2015**, *353*, 530–539. [[CrossRef](#)]
6. Zhang, W.; Dehghani-Sanij, A.A.; Blackburn, R.S. Carbon based conductive polymer composites. *J. Mater. Sci.* **2007**, *42*, 3408–3418. [[CrossRef](#)]
7. Manjaly Poulouse, A.; Anis, A.; Shaikh, H.; George, J.; Al-Zahrani, S.M. Effect of plasticizer on the electrical, thermal, and morphological properties of carbon black filled poly(propylene). *Polym. Compos.* **2017**, *38*, 2472–2479. [[CrossRef](#)]
8. Andrews, R.; Weisenberger, M. Carbon nanotube polymer composites. *Curr. Opin. Solid State Mater. Sci.* **2004**, *8*, 31–37. [[CrossRef](#)]
9. Du, J.; Cheng, H.-M. The Fabrication, Properties, and Uses of Graphene/Polymer Composites. *Macromol. Chem. Phys.* **2012**, *213*, 1060–1077. [[CrossRef](#)]
10. Feih, S.; Mouritz, A.P. Tensile properties of carbon fibres and carbon fibre–polymer composites in fire. *Compos. Part A Appl. Sci. Manuf.* **2012**, *43*, 765–772. [[CrossRef](#)]
11. de Souza Vieira, L.; dos Anjos, E.G.R.; Verginio, G.E.A.; Oyama, I.C.; Braga, N.F.; da Silva, T.F.; Montagna, L.S.; Rezende, M.C.; Passador, F.R. Carbon-based materials as antistatic agents for the production of antistatic packaging: A review. *J. Mater. Sci. Mater. Electron.* **2021**, *32*, 3929–3947. [[CrossRef](#)]
12. Ferreira, G.F.; Pierozzi, M.; Fingolo, A.C.; da Silva, W.P.; Strauss, M. Tuning sugarcane bagasse biochar into a potential carbon black substitute for polyethylene composites. *J. Polym. Environ.* **2019**, *27*, 1735–1745. [[CrossRef](#)]
13. Peterson, S.C. Utilization of low-ash biochar to partially replace carbon black in styrene–butadiene rubber composites. *J. Elastomers Plast.* **2013**, *45*, 487–497. [[CrossRef](#)]
14. Das, O.; Sarmah, A.K.; Bhattacharyya, D. Biocomposites from waste derived biochars: Mechanical, thermal, chemical, and morphological properties. *Waste Manag.* **2016**, *49*, 560–570. [[CrossRef](#)] [[PubMed](#)]
15. Das, O.; Sarmah, A.K. Mechanism of waste biomass pyrolysis: Effect of physical and chemical pre-treatments. *Sci. Total Environ.* **2015**, *537*, 323–334. [[CrossRef](#)] [[PubMed](#)]
16. Das, S.K.; Ghosh, G.K.; Avasthe, R.K.; Sinha, K. Compositional heterogeneity of different biochar: Effect of pyrolysis temperature and feedstocks. *J. Environ. Manag.* **2021**, *278*, 111501. [[CrossRef](#)] [[PubMed](#)]
17. Fingolo, A.C.; Bettini, J.; Cavalcante, M.S.; Pereira, M.P.; Bufon, C.C.B.; Santhiago, M.; Strauss, M. Boosting Electrical Conductivity of Sugarcane Cellulose and Lignin Biocarbons through Annealing under Isopropanol Vapor. *ACS Sustain. Chem. Eng.* **2020**, *8*, 7002–7010. [[CrossRef](#)]
18. Poulouse, A.M.; Elnour, A.Y.; Anis, A.; Shaikh, H.; Al-Zahrani, S.M.; George, J.; Al-WabelAdel, M.I.; Usman, R.; Ok, Y.S.; Tsang, D.C.W.; et al. Date palm biochar-polymer composites: An investigation of electrical, mechanical, thermal and rheological characteristics. *Sci. Total Environ.* **2018**, *619*, 311–318. [[CrossRef](#)]
19. Das, O.; Sarmah, A.K.; Bhattacharyya, D. A sustainable and resilient approach through biochar addition in wood polymer composites. *Sci. Total Environ.* **2015**, *512*, 326–336. [[CrossRef](#)]
20. Das, O.; Sarmah, A.K.; Bhattacharyya, D. Structure–mechanics property relationship of waste derived biochars. *Sci. Total Environ.* **2015**, *538*, 611–620. [[CrossRef](#)]
21. Monteiro, S.N.; Monteiro, S.N.; Calado, V.; Rodriguez, R.J.S.; Margem, F.M. Thermogravimetric stability of polymer composites reinforced with less common lignocellulosic fibers—An Overview. *J. Mater. Res. Technol.* **2012**, *1*, 117–126. [[CrossRef](#)]
22. Das, O.; Sarmah, A.K. The love–hate relationship of pyrolysis biochar and water: A perspective. *Sci. Total Environ.* **2015**, *512*, 682–685. [[CrossRef](#)] [[PubMed](#)]
23. Nan, N.; DeVallance, D.B.; Xie, X.; Wang, J. The effect of bio-carbon addition on the electrical, mechanical, and thermal properties of polyvinyl alcohol/biochar composites. *J. Compos. Mater.* **2016**, *50*, 1161–1168. [[CrossRef](#)]
24. Alwasitti, A.A.; Al-Zubaidi, N.S.; Salam, M. Enhancing lubricity of drilling fluid using nanomaterial additives. *Pet. Coal* **2019**, *61*, 467–469.

25. Jayabalakrishnan, D.; Prabhu, P.; Iqbal, M.S.; Mugendiran, V.; Ravi, S.; Prakash, A.V.R. Mechanical, dielectric, and hydrophobicity behavior of coconut shell biochar toughened *Caryota urens* natural fiber reinforced epoxy composite. *Polym. Compos.* **2022**, *43*, 493–502.
26. Jain, A.; Aravindan, V.; Jayaraman, S.; Kumar, P.S.; Balasubramanian, R.; Ramakrishna, S.; Madhavi, S.; Srinivasan, M.P. Activated carbons derived from coconut shells as high energy density cathode material for Li-ion capacitors. *Sci. Rep.* **2013**, *3*, 3002. [[CrossRef](#)]
27. Amuda, O.; Giwa, A.; Bello, I. Removal of heavy metal from industrial wastewater using modified activated coconut shell carbon. *Biochem. Eng. J.* **2007**, *36*, 174–181. [[CrossRef](#)]
28. Freitas, J.V.; Nogueira, F.G.; Farinas, C.S. Coconut shell activated carbon as an alternative adsorbent of inhibitors from lignocellulosic biomass pretreatment. *Ind. Crops Prod.* **2019**, *137*, 16–23. [[CrossRef](#)]
29. Abe, I.; Fukuhara, T.; Maruyama, J.; Tatsumoto, H.; Iwasaki, S. Preparation of carbonaceous adsorbents for removal of chloroform from drinking water. *Carbon* **2001**, *39*, 1069–1073. [[CrossRef](#)]
30. Bartoli, M.; Giorcelli, M.; Jagdale, P.; Rovere, M.; Tagliaferro, A. A review of non-soil biochar applications. *Materials* **2020**, *13*, 261. [[CrossRef](#)]
31. Nagarajan, V.; Mohanty, A.K.; Misra, M. Biocomposites with size-fractionated biocarbon: Influence of the microstructure on macroscopic properties. *ACS Omega* **2016**, *1*, 636–647. [[CrossRef](#)]
32. Das, O.; Bhattacharyya, D.; Hui, D.; Lau, K. Mechanical and flammability characterisations of biochar/polypropylene biocomposites. *Compos. Part B Eng.* **2016**, *106*, 120–128. [[CrossRef](#)]
33. Umerah, C.O.; Kodali, D.; Head, S.; Jeelani, S.; Rangari, V.K. Synthesis of carbon from waste coconutshell and their application as filler in bioplast polymer filaments for 3D printing. *Compos. Part B Eng.* **2020**, *202*, 108428. [[CrossRef](#)]
34. Husain, Z.; Raheman, A.R.S.; Ansari, K.B.; Pandit, A.B.; Khan, M.S.; Qyyum, M.A.; Lam, S.S. Nano-sized mesoporous biochar derived from biomass pyrolysis as electrochemical energy storage supercapacitor. *Mater. Sci. Energy Technol.* **2022**, *5*, 99–109. [[CrossRef](#)]
35. Żenkiewicz, M.; Richert, J.; Rytlewski, P.; Richert, A. Comparative analysis of shungite and graphite effects on some properties of polylactide composites. *Polym. Test.* **2011**, *30*, 429–435. [[CrossRef](#)]
36. Al-Itry, R.; Lamnawar, K.; Maazouz, A. Rheological, morphological, and interfacial properties of compatibilized PLA/PBAT blends. *Rheol. Acta* **2014**, *53*, 501–517. [[CrossRef](#)]
37. Sarul, D.S.; Arslan, D.; Vatanserver, E.; Kahraman, Y.; Durmus, A.; Salehiyan, R.; Nofar, M. Preparation and characterization of PLA/PBAT/CNC blend nanocomposites. *Colloid Polym. Sci.* **2021**, *299*, 987–998. [[CrossRef](#)]
38. Urquijo, J.; Aranburu, N.; Dagr eou, S.; Guerrica-Echevarr a, G.; Eguiaz abal, J.I. CNT-induced morphology and its effect on properties in PLA/PBAT-based nanocomposites. *Eur. Polym. J.* **2017**, *93*, 545–555. [[CrossRef](#)]
39. Benwood, C.; Anstey, A.; Andrzejewski, J.; Misra, M.; Mohanty, A.K. Improving the impact strength and heat resistance of 3D printed models: Structure, property, and processing correlations during fused deposition modeling (FDM) of poly (lactic acid). *ACS Omega* **2018**, *3*, 4400–4411. [[CrossRef](#)]
40. Wootthikanokkhan, J.; Cheachun, T.; Sombatsompop, N.; Thumsorn, S.; Kaabbuathong, N.; Wongta, N.; Wong-On, J.; Ayutthaya, S.I.N.; Kositchaiyong, A. Crystallization and thermomechanical properties of PLA composites: Effects of additive types and heat treatment. *J. Appl. Polym. Sci.* **2013**, *129*, 215–223. [[CrossRef](#)]
41. Zhou, S.-Y.; Huang, H.-D.; Ji, X.; Yan, D.-X.; Zhong, G.-J.; Hsiao, B.S.; Li, Z.-M. Super-Robust Polylactide Barrier Films by Building Densely Oriented Lamellae Incorporated with Ductile in Situ Nanofibrils of Poly(butylene adipate-co-terephthalate). *ACS Appl. Mater. Interfaces* **2016**, *8*, 8096–8109. [[CrossRef](#)]
42. George, J.; Azad, L.B.; Poulouse, A.M.; An, Y.; Sarmah, A.K. Nano-mechanical behaviour of biochar-starch polymer composite: Investigation through advanced dynamic atomic force microscopy. *Compos. Part A Appl. Sci. Manuf.* **2019**, *124*, 105486. [[CrossRef](#)]
43. Al-Wabel, M.I.; Al-Omran, A.; El-Naggar, A.H.; Nadeem, M.; Usman, A.R.A. Pyrolysis temperature induced changes in characteristics and chemical composition of biochar produced from *Conocarpus* wastes. *Bioresour. Technol.* **2013**, *131*, 374–379. [[CrossRef](#)] [[PubMed](#)]
44. Mishra, A.K.; Ramaprabhu, S. Carbon dioxide adsorption in graphene sheets. *AIP Adv.* **2011**, *1*, 032152. [[CrossRef](#)]
45. Idrees, M.; Jeelani, S.; Rangari, V. Three-dimensional-printed sustainable biochar-recycled PET composites. *ACS Sustain. Chem. Eng.* **2018**, *6*, 13940–13948. [[CrossRef](#)]
46. Zhao, C.; Wang, Q.; Lu, Y.; Li, B.; Chen, L.; Hu, Y.-S. High-temperature treatment induced carbon anode with ultrahigh Na storage capacity at low-voltage plateau. *Sci. Bull.* **2018**, *63*, 1125–1129. [[CrossRef](#)]
47. Qian, K.; Kumar, A.; Zhang, H.; Bellmer, D.; Huhnke, R. Recent advances in utilization of biochar. *Renew. Sustain. Energy Rev.* **2015**, *42*, 1055–1064. [[CrossRef](#)]
48. Harris, A.M.; Lee, E.C. Improving mechanical performance of injection molded PLA by controlling crystallinity. *J. Appl. Polym. Sci.* **2008**, *107*, 2246–2255. [[CrossRef](#)]
49. Ikram, S.; Das, O.; Bhattacharyya, D. A parametric study of mechanical and flammability properties of biochar reinforced polypropylene composites. *Compos. Part A Appl. Sci. Manuf.* **2016**, *91*, 177–188. [[CrossRef](#)]
50. Scaffaro, R.; Botta, L.; Lopresti, F.; Maio, A.; Suter, F. Polysaccharide nanocrystals as fillers for PLA based nanocomposites. *Cellulose* **2017**, *24*, 447–478. [[CrossRef](#)]

51. Xiao, H.; Lu, W.; Yeh, J.T. Crystallization behavior of fully biodegradable poly (lactic acid)/poly (butylene adipate-co-terephthalate) blends. *J. Appl. Polym. Sci.* **2009**, *112*, 3754–3763. [[CrossRef](#)]
52. Yeh, J.T.; Yeh, J.-T.; Tsou, C.-H.; Huang, C.-Y.; Chen, K.-N.; Wu, C.-S.; Chai, W.-L. Compatible and crystallization properties of poly (lactic acid)/poly (butylene adipate-co-terephthalate) blends. *J. Appl. Polym. Sci.* **2010**, *116*, 680–687. [[CrossRef](#)]
53. Lu, X.; Zhao, J.; Yang, X.; Xiao, P. Morphology and properties of biodegradable poly (lactic acid)/poly (butylene adipate-co-terephthalate) blends with different viscosity ratio. *Polym. Test.* **2017**, *60*, 58–67. [[CrossRef](#)]
54. Al-Itry, R.; Lamnawar, K.; Maazouz, A. Improvement of thermal stability, rheological and mechanical properties of PLA, PBAT and their blends by reactive extrusion with functionalized epoxy. *Polym. Degrad. Stab.* **2012**, *97*, 1898–1914. [[CrossRef](#)]
55. George, J.; Bhattacharyya, D. Biocarbon reinforced polypropylene composite: An investigation of mechanical and filler behavior through advanced dynamic atomic force microscopy and X-ray micro CT. *Express Polym. Lett.* **2021**, *15*, 224–235. [[CrossRef](#)]
56. Musioł, M.; Rydz, J.; Janeczek, H.; Kordyka, A.; Andrzejewski, J.; Sterzyński, T.; Jurczyk, S.; Cristea, M.; Musioł, K.; Kampik, M.; et al. (Bio)degradable biochar composites—Studies on degradation and electrostatic properties. *Mater. Sci. Eng. B* **2022**, *275*, 115515. [[CrossRef](#)]
57. Markarian, J. New developments in antistatic and conductive additives. *Plast. Addit. Compd.* **2008**, *10*, 22–25. [[CrossRef](#)]
58. Mojzes, A.; Tóth, B.; Csavajda, P. Investigation of an electrostatic discharge protective biodegradable packaging foam in the logistic chain. *Logist. Sustain. Transp.* **2014**, *5*, 25–33. [[CrossRef](#)]
59. Gabhi, R.; Basile, L.; Kirk, D.W.; Giorcelli, M.; Tagliaferro, A.; Jia, C.Q. Electrical conductivity of wood biochar monoliths and its dependence on pyrolysis temperature. *Biochar* **2020**, *2*, 369–378. [[CrossRef](#)]
60. Gabhi, R.S.; Kirk, D.W.; Jia, C.Q. Preliminary investigation of electrical conductivity of monolithic biochar. *Carbon* **2017**, *116*, 435–442. [[CrossRef](#)]
61. Guo, Y.; Zuo, X.; Xue, Y.; Zhou, Y.; Yang, Z.; Chuang, Y.-C.; Chang, C.-C.; Yuan, G.; Satija, S.K.; Gersappe, D.; et al. Enhancing impact resistance of polymer blends via self-assembled nanoscale interfacial structures. *Macromolecules* **2018**, *51*, 3897–3910. [[CrossRef](#)]
62. Deng, Y.; Yu, C.; Wongwiwattana, P.; Thomas, N.L. Optimising Ductility of Poly(Lactic Acid)/Poly(Butylene Adipate-co-Terephthalate) Blends Through Co-continuous Phase Morphology. *J. Polym. Environ.* **2018**, *26*, 3802–3816. [[CrossRef](#)]
63. Salehiyan, R.; Nofar, M.; Malkappa, K.; Ray, S.S. Effect of nanofillers characteristics and their selective localization on morphology development and rheological properties of melt-processed polylactide/poly (butylene adipate-co-terephthalate) blend composites. *Polym. Eng. Sci.* **2020**, *60*, 2749–2760. [[CrossRef](#)]
64. Ding, Y.; Zhang, C.; Luo, C.; Chen, Y.; Zhou, Y.; Yao, B.; Dong, L.; Du, X.; Ji, J. Effect of talc and diatomite on compatible, morphological, and mechanical behavior of PLA/PBAT blends. *e-Polymers* **2021**, *21*, 234–243. [[CrossRef](#)]
65. Ko, S.; Hong, M.K.; Park, B.J.; Gupta, R.K.; Choi, H.J.; Bhattacharya, S.N. Morphological and rheological characterization of multi-walled carbon nanotube/PLA/PBAT blend nanocomposites. *Polym. Bull.* **2009**, *63*, 125–134. [[CrossRef](#)]
66. Giorcelli, M.; Khan, A.; Pugno, N.M.; Rosso, C.; Tagliaferro, A. Biochar as a cheap and environmental friendly filler able to improve polymer mechanical properties. *Biomass Bioenergy* **2019**, *120*, 219–223. [[CrossRef](#)]
67. Suryanegara, L.; Nakagaito, A.N.; Yano, H. The effect of crystallization of PLA on the thermal and mechanical properties of microfibrillated cellulose-reinforced PLA composites. *Compos. Sci. Technol.* **2009**, *69*, 1187–1192. [[CrossRef](#)]
68. Meng, H.; Meng, H.; Sui, G.X.; Fang, P.F.; Yang, R. Effects of acid-and diamine-modified MWNTs on the mechanical properties and crystallization behavior of polyamide 6. *Polymer* **2008**, *49*, 610–620. [[CrossRef](#)]

Disclaimer/Publisher’s Note: The statements, opinions and data contained in all publications are solely those of the individual author(s) and contributor(s) and not of MDPI and/or the editor(s). MDPI and/or the editor(s) disclaim responsibility for any injury to people or property resulting from any ideas, methods, instructions or products referred to in the content.